Ionic Channel Structures in $[(M^+)_x([18]crown\text{-}6)][Ni(dmit)_2]_2$ Molecular Conductors**

Tomoyuki Akutagawa,*[a, b] Tatsuo Hasegawa,[a] Takayoshi Nakamura,*[a] Sadamu Takeda,[c] Tamotsu Inabe,[c] Ken-ichi Sugiura,[d] Yoshiteru Sakata,[d] and Allan E. Underhill[e]

Abstract: The $[(M^+)_x([18]crown\text{-}6)]$ supramolecular cations (SC^+), in which M^+ and [18]crown-6 are alkali metal ions ($M^+ = Li^+$, Na^+, and Cs^+) and 1,4,7,10,13,16-hexaoxacyclooctadecane, respectively, form ionic channel structures through the regular stacks of [18]crown-6 in $[Ni(dmit)_2]$-based molecular conductors ($dmit^{2-}$ = 2-thioxo-1,3-dithiole-4,5-dithiolate). In addition to the $[Ni(dmit)_2]$ salts that have the ionic channel structures (these salts are abbreviated as type **I** salts), Li^+ and Na^+ form dimerized $[(M^+)_2([18]crown\text{-}6)_2]$ units in the crystals (type **II** salts). The K^+ and Rb^+ are coordinated tightly into the [18]crown-6 cavity to form typical disk-shape SC^+ units in the corresponding $[Ni(dmit)_2]$ salts (type **III** salts). The type **I**, **II**, and **III** salts have typical stoichiometries of $[(M^+)_x([18]crown\text{-}6)][Ni(dmit)_2]_2$, $[(M^+)([18]crown\text{-}6)(H_2O)_x(CH_3CN)_{1.5-x}][Ni(dmit)_2]_3$ ($x = 1$ for Li^+ or 0.5 for Na^+), and $[M^+([18]crown\text{-}6)][Ni(dmit)_2]_3$, respectively; the salts of the same type are isostructural. In agreement with the trimer structures of $[Ni(dmit)_2]$ in the type **II** and **III** salts, they exhibit semiconducting behavior with electrical conductivities at 300 K ($\sigma_{300\,K}$) of $0.01-0.1\ S\,cm^{-1}$. Type **I** salts contain a regular stack of partially oxidized $[Ni(dmit)_2]$ units, which form a quasi one-dimensional metallic band within the tight-binding approximation regime. The electrical conductivities at 300 K are $10-30\ S\,cm^{-1}$, and an almost temperature-independent conductivity was observed at higher temperatures. However, the one-dimensional electronic structures in these salts are strongly influenced by the static and dynamic structures of the coexisting ionic channel. The Na^+ salt is a semiconductor, whose magnetic behavior is described by the disordered one-dimensional antiferromagnetic chain. On the other hand, the Cs^+ salt is a exhibits metallic properties with $2k_F$ instability at room temperature. The Li^+ salt shows a gradual transition from the high-temperature metallic phase to the low-temperature one-dimensional antiferromagnetic semiconductor phase, which was associated with the freezing of Li^+ motion at lower temperatures. The preferential crystallization of type **I** salts was possible by controlling the equilibrium constant (K_c) of the complex formation between M^+ ions and the [18]crown-6 molecule. The ionic channel structures were obtained when the K_c was low in the electrocrystallization solution, while type **II** or **III** salts were formed in the high K_c region.

Keywords: conducting materials · crystal engineering · ionic channels · structure elucidation · supramolecular chemistry

[a] Dr. T. Akutagawa, Prof. T. Nakamura, Prof. T. Hasegawa
Research Institute for Electronic Science
Hokkaido University, Sapporo 060-0812 (Japan)
Fax: (+81) 11-706-4972
E-mail: takuta@imd.es.hokudai.ac.jp

[b] Dr. T. Akutagawa
PRESTO
Japan Science and Technology Corporation (Japan)

[c] Prof. S. Takeda, Prof. T. Inabe
Department of Chemistry, Faculty of Science
Hokkaido University, Sapporo 060-0810 (Japan)

[d] Dr. K.-i. Sugiura, Prof. Y. Sakata
Institute of Scientific and Industrial Research
Osaka University, Ibaraki, Osaka 567-0047 (Japan)

[e] Prof. A. E. Underhill
Department of Chemistry, University of Wales
Bangor, Gwynedd LL57 3UW (UK)

Supporting information for this article is available on the WWW under http://www.wiley-vch.de/home/chemistry/ or from the author.

[**] Nomenclature used in this paper: Since one $dmit^{2-}$ ligand has the formal charge of $2-$, the total charge of closed-shell initial state of $[Ni(dmit)_2]$ is $2-$. On the other hand, the $[Ni(dmit)_2]$ molecule has two-step redox processes from $[Ni(dmit)_2]^{2-}$, $[Ni(dmit)_2]^-$ to $[Ni(dmit)_2]^0$. From the molecular orbital calculation of $[Ni(dmit)_2]$, the ligand p orbital mainly contributes to the HOMO and LUMO of $[Ni(dmit)_2]$ molecule. Thus, the oxidation processes of $[Ni(dmit)_2]$ molecule mainly occurs at the ligand, withholding the Ni^{2+} charge. Within the salts labeled throughout this paper as $[(M^+)_x([18]crown\text{-}6)][Ni(dmit)_2]_2$ or $[M^+([18]crown\text{-}6)][Ni(dmit)_2]_3$, the $[Ni(dmit)_2]$ anion exists as partially charge-transferred state. The average charged state of $[Ni(dmit)_2]$ in these salts can be represented as $[M_x([18]crown\text{-}6)]^+2[Ni(dmit)_2]^{0.5-}$ and $[M([18]crown\text{-}6)]^+3[Ni(dmit)_2]^{0.33-}$, respectively.

  0947-6539/01/0722-4902 $ 17.50+.50/0

Introduction

Ionic channels are one of the important biological elements in the cell membranes of nerves, muscles, and synapses.[1] They often play an important role in the assertion of fundamental biological functions, such as ion-pumping in ATPase and generation of action potential for signal transmission.[1, 2] The ion transport in biological cell membranes is precisely controlled by the opening and closing of ionic channels, and this gating mechanism is governed by the cooperative electronic processes in ATPase.[1, 2] There are several kinds of approaches for constructing artificial ionic channel structures. One method utilizes the helical oligopeptide structure in natural-cell ionic channels.[3] The other method is based on completely artificial synthetic organic molecules, such as crown ethers:[4] crown ethers can selectively include ions in their cavities.[5] Cation transport through the ionic channel has been reported in which the selective ion diffusion is mediated by the array of crown ethers across the lipid bilayer membrane.[4]

The formation of artificial ionic channel structures in the crystalline solid has been reported by a number of groups who aimed to construct molecular ionic devices.[6, 7] However, an artificial ionic channel whose ion transport is coupled with electronic processes has not been established to our knowledge. We are interested in constructing integrated molecular systems with ionic channels and electronic conductors by forming hybrid compounds of crown-ether-based molecular assemblies with molecular conductors. In such systems, the electronic state of the molecular conductors should be affected by the dynamic motion of the ions. We can also expect novel functions arising from the cooperative processes of ions and electrons in the system.

A large number of molecular conductors based on radical cation or anion salts have been reported.[8] These crystals are composed of open-shell electron donor (or acceptor) molecules and closed-shell counterions X^- (or cations C^+); the latter species neutralize the charge on the open-shell molecules. The open-shell molecules are stacked in the crystal to form electronic π-band structures.[8] As a consequence of the low-dimensional nature of the conduction π bands, the electronic system is influenced by the counterions within the crystal lattice. The electronic transitions caused by the dynamics of ionic lattice are often observed, for example, i) metal–insulator transition through the ordering of tetrahedral anions (formation of a superlattice)[9] or the magnetic ordering of counteranion columns,[10] ii) ferromagnetic spin ordering of counterions in the metallic state,[11] and iii) superconductor–insulator transition induced by antiferromagnetic d–π coupling of the counterions.[12] The periodicity of counterions in the crystal lattice is conserved during these transitions, and small modifications in the ionic lattice are responsible for the large changes in conductivity. By combining the molecular conductors with ionic channels in which ions have larger motional freedom, it should be possible to control the electronic transport by a regulation of the ion dynamics within the ionic channel. The cooperative ion–electron transport in such systems should exhibit novel "switching" in electrical conductivity and magnetism according to the magnitude of the interaction between the ion and electron. This is a promising basis for the construction of future iono-electronic devices.[4]

Several attempts have been made to incorporate supramolecular cation (SC^+) structures into molecular conductors in order to construct molecular iono-electronic devices.[13, 14] The SC^+ structures based on crown ethers have been succesfully incorporated into the anion radical salt of 7,7,8,8-tetracyanoquinodimethane (TCNQ),[13, 14] although ionic channel structures were not realized. The crown-ether-fused phthalocyanine (Pc) molecules have also been reported as a supramolecular ion–electron cooperative system.[15] The electrical conductivity of the Pc system was tuned through the cation-binding in the crown ether moieties. However, the electronic systems of these TCNQ and Pc compounds are essentially semiconducting or insulating.

The nickel dithiolate complex $[Ni(dmit)_2]$ ($dmit^{2-}$ = 2-thioxo-1,3-dithiole-4,5-dithiolate) is an appropriate electron acceptor for these SC^+ hybrid systems.[16a] The π–π stacks of the partially oxidized $[Ni(dmit)_2]$ exhibit high electrical conductivity along the π-stacking direction down to low temperatures.[8b][16, 17] We have already reported several model systems of electrically conducting $SC^+[Ni(dmit)_2]_x$ salts.[16] Most of the SCs have isolated ion-capturing cavities rather than an ionic channel structure. One exception is the ionic channel structure observed in highly conducting $[(Li^+)_{0.6}([15]\text{-crown-5})(H_2O)][Ni(dmit)_2]_2$ salt, which has an electrical conductivity of 250 $S\,cm^{-1}$ at 300 K.[17] However, the strategy for designing the ionic channel structure within the $[Ni(dmit)_2]$-based molecular conductor is not yet clear. Here we report a new series of $[(M^+)_x([18]\text{crown-6}][Ni(dmit)_2]_y$ mo-

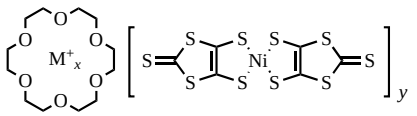

$[(M^+)_x([18]\text{crown-6})][Ni(dmit)_2]_y$

I: $x<1$, $y=2$
II and **III**: $x=1$, $y=3$

lecular conductors (M^+ = Li^+, Na^+, K^+, Rb^+, and Cs^+), including highly conducting salts with new ionic channel structures. We succeeded in the preferential formation of ionic channel structures within the crystal by controlling the complex formation constant between alkali metal cations and [18]crown-6 in solution. The salts exhibit a semimetallic behavior at higher temperatures. Their electronic and magnetic behavior is explained in terms of the interplay between the motional freedom of ions within the channel and the conduction of electrons in the $[Ni(dmit)_2]$ stack.

Results and Discussion

Crystal structure: Table 1 summarizes the crystal types (see below), stoichiometry, crystal shape, and electrocrystallization solvent of seven new $[Ni(dmit)_2]$ salts (**1a**–**5**). Ionic channel structures were obtained for the Li^+ (**1a**), Na^+ (**2a**), and Cs^+

  0947-6539/01/0722-4903 $ 17.50+.50/0

Table 1. Type of crystal, stoichiometry, crystal shape, and electrocrystallization solvent of the salts **1**–**5**.

	Type[a]	Stoichiometry[b]	Shape	Solvent[c]
1a	**I**	$[(Li^+)_{0.42}([18]crown-6)][Ni(dmit)_2]_2$[d]	thin plate	CH_3CN/H_2O
1b	**II**	$[(Li^+)([18]crown-6)(H_2O)(CH_3CN)_{0.5}][Ni(dmit)_2]_3$	plate	CH_3CN
2a	**I**	$[(Na^+)_{0.66}([18]crown-6)][Ni(dmit)_2]_2(H_2O)$	needle	CH_3CN/H_2O
2b	**II**	$[(Na^+)([18]crown-6)(H_2O)_{0.5}(CH_3CN)][Ni(dmit)_2]_3$	plate	CH_3CN
3	**III**	$[(K^+)([18]crown-6)][Ni(dmit)_2]_3$	plate	CH_3CN
4	**III**	$[(Rb^+)([18]crown-6)][Ni(dmit)_2]_3$	plate	CH_3CN
5	**I**	$[(Cs^+)_{0.8}([18]crown-6)][Ni(dmit)_2]_2$	fine needle	CH_3CN

[a] See text. [b] Determined by X-ray crystal structural analysis. [c] Mixed solvent system was employed for the crystal preparations of the salts **1a** and **2a** with CH_3CN/H_2O 9:1. [d] Li^+ stoichiometry was determined by the temperature-dependent magnetic susceptibility.

(**5**) salts. The salts have typical stoichiometries of $[(M^+)_x([18]crown-6)][Ni(dmit)_2]_2$. Hereafter, we abbreviate these salts as type **I**. In the case of Li^+ and Na^+, $[(M^+)([18]crown-6)(H_2O)_x(CH_3CN)_{1.5-x}][Ni(dmit)_2]_3$ salts were also obtained; these contain dimerized $\{(M^+)_2([18]crown-6)_2\}$ units in the crystal (type **II**). K^+ and Rb^+ gave type **III** salts with typical stoichiometries of $[(M^+)([18]crown-6)][Ni(dmit)_2]_3$; these have an isolated disk-shape SC^+ unit of $[(M^+)([18]crown-6)]$. The salts of the same type are isostructural.

In all cases, the $[Ni(dmit)_2]$ columns are arranged into a two-dimensional layer through side-by-side S···S interatomic contacts, while the SC^+ units are located in the cavities between the $[Ni(dmit)_2]$ layers. The conducting columns of the type **I** salts are composed of a $[Ni(dmit)_2]$ uniform stack, while the $[Ni(dmit)_2]$ anions in the type **II** and **III** salts form trimeric units. The structural details of the $[Ni(dmit)_2]$ layers and SC^+ units are described below (Table 2).

Crystal structure of type I salts: Figures 1a and b show the unit cell of the salt **1a** viewed along the *a* and *b* axes, respectively. Both the $[Ni(dmit)_2]$ anions and the $[(Li^+)_x([18]crown-6)]$ units are stacked uniformly along the *a* axis, and the regular array of the [18]crown-6 molecules forms an ionic channel structure along the *a* axis. No intermolecular $Li^+\cdots S$ contacts were observed.

The intracolumn transfer integral ($t_1 \times 10^{-2}$ eV) of salt **1a** is 12.8 (Figure 1c); this value is close to that in the superconductor of $(CH_3)_4N[Ni(dmit)_2]_2$ ($t = 10.2$ and -10.8).[18] On the other hand, the intercolumn interactions (t_4 and t_5), which are $\approx$40 times smaller than t_1, are not effective for increasing electronic dimensionality of the $[Ni(dmit)_2]$ layer (Table 2). Figure 1d shows the band structure and the Fermi surface of salt **1a**. The LUMO band is slightly split into two because of the t_4 and t_5 interactions. The dispersion of the LUMO band is only observed along the X direction. The highly one-dimensional electronic structure is caused by the LUMO symmetry (b_{2g}), which is not suitable for increasing side-by-side transverse interactions compared with the HOMO of the TTF analogues (b_{1u} symmetry).[8][19]

Ionic channel structure: Although the type **I** salts are isostructural, the ionic channel structures differ according to the size of the ions within the channel: i) The Li^+ ions are much smaller than the cavity size of [18]crown-6, and have two disordered ionic sites above and below the [18]crown-6 plane (Figure 2a). ii) The Na^+ ion is slightly smaller than the [18]crown-6 cavity and is completely included within the [18]crown-6 cavity. The water molecules are located at the inversion center and connect the $\{(Na^+)_{0.66}([18]crown-6)\}$ units (Figure 2b). iii) The Cs^+ ion is too large to be included in the cavity and is located at the inversion center between two [18]crown-6 molecules (Figure 2c). It should be noted that we could not obtain type **I** salts for K^+ and Rb^+ ions, whose size fits well to the cavity of [18]crown-6.

The occupancy factor of Na^+ and Cs^+ within the channel is less than unity with the occupancy factors of 0.66 (**2a**) and 0.8 (**5**), respectively. The number of Li^+ ions in the crystal, which corresponds to the spin number observed in magnetic susceptibility measurements (see below), is about 0.21 per site. Therefore, the average charge on $[Ni(dmit)_2]$ is -0.21, -0.33, and -0.40 for the Li^+, Na^+, and Cs^+ salts, respectively. The vacant ionic sites within the channel imply the motional freedom of smaller ions, such as Li^+ and Na^+, within the channel, while the Cs^+ ion is too large to pass through the [18]crown-6 cavity.

The average $Li^+\cdots O$ distance (2.82 Å) found in the salt **1a** is $\approx$0.7 Å longer than the sum of the van der Waals radi of the oxygen atom and the ionic radius of Li^+.[20] The Li^+ ions in the salt **1a** are not rigidly

Table 2. Structural parameters of $[Ni(dmit)_2]$ layer and SC^+ unit. Transfer integrals ($t \times 10^{-2}$ eV) within the $[Ni(dmit)_2]$ layer[a] and average $M^+\cdots O$ contacts ($M^+\cdots O_{av}$), average isotropic thermal parameter (B), and COC asymmetric stretching frequency (ν^a_{COC} [cm^{-1}]) within the SC^+ units.

	Type **I**			Type **II**		Type **III**	
	1a	**2a**	**5**	**1b**	**2b**	**3**	**4**
t_1	12.8	13.36	13.5	15.17	−17.20	−15.3	−15.3
t_2	–	–	–	−0.89	−0.23	−3.70	−3.04
t_3	–	–	–	14.83	−16.26	3.55	3.40
t_4	−0.27	−0.62	−0.40	−0.45	−0.33	−0.06	−0.11
$t_{4'}$	–	–	–	−0.25	−0.02	–	–
t_5	0.18	0.40	0.32	2.62	0.39	1.32	1.50
$t_{5'}$	–	–	–	−0.58	1.26	–	–
t_6	–	–	–	0.24	−0.54	−0.67	−0.54
$t_{6'}$	–	–	–	−0.37	−0.50	–	–
t_7	–	–	–	−0.92	1.80	–	–
$t_{7'}$	–	–	–	0.17	−5.86	–	–
$M^+\cdots O_{av}$	2.82	2.75	3.58	2.09	2.75	2.80	2.86
B	6.9	9.0	9.0	5.3	10.1	4.4	4.9
ν^a_{COC}	1103	1109	1105	1105	1111	1102	1098

[a] The transfer integrals (t) were calculated from the LUMO of $[Ni(dmit)_2]$ molecule based on the extended Hückel calculation ($t = -10\,S$ eV, S is the overlap integral).

0947-6539/01/0722-4904 $ 17.50+.50/0 *Chem. Eur. J.* **2001**, *7*, No. 22

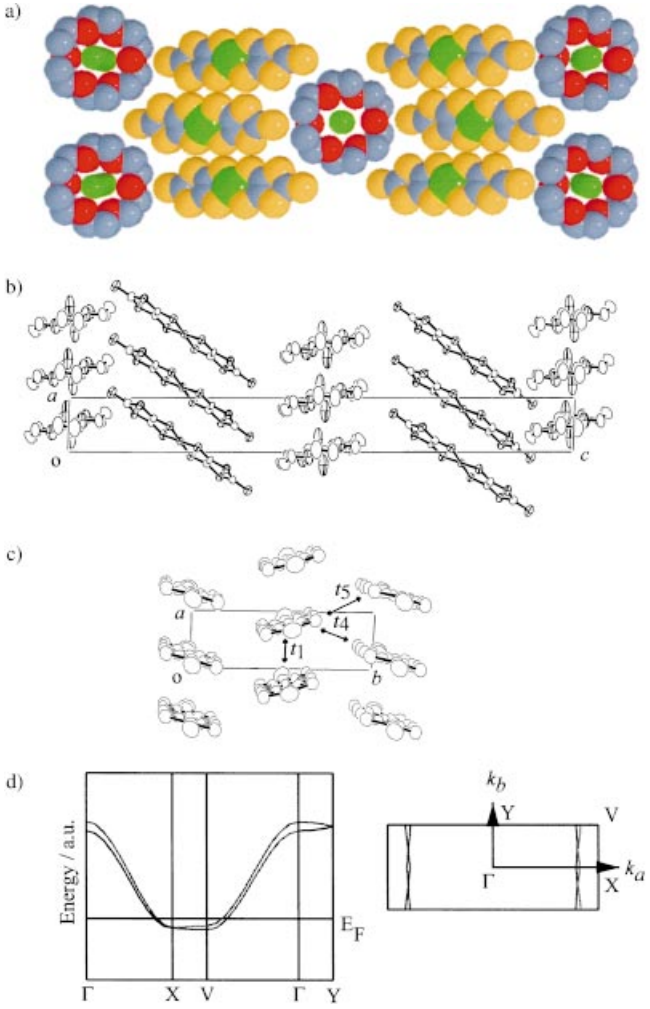

Figure 1. Crystal structure of $[(Li^+)_x([18]crown\text{-}6)][Ni(dmit)_2]_2$ (**1a**). a) Unit cell viewed along the *a* axis and b) along the *b* axis. c) Transfer integrals ($t \times 10^{-2}$ eV) within the $[Ni(dmit)_2]$ layer viewed along the long axis of the $[Ni(dmit)_2]$ molecule. d) The energy dispersion (left) and Fermi surface (right) of the LUMO band. The Γ, X, V, and Y points are (0, 0, 0), (1, 0, 0), (1, 1, 0), and (0, 1, 0), respectively.

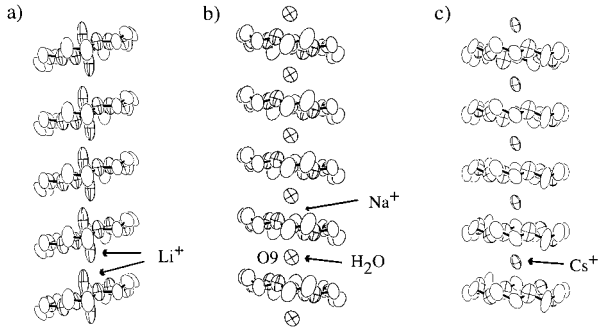

Figure 2. Ionic channel structures found in the type **I** salt viewed normal to the stacking direction. a) $[(Li^+)_x([18]crown\text{-}6)]$ units with the two positionally disordered M^+ sites (above and below the [18]crown-6 plane). b) $[(Na^+)_{0.66}([18]crown\text{-}6)(H_2O)]$ units in which the Na^+ ion locates at the center of the cavity. c) $[(Cs^+)_{0.8}([18]crown\text{-}6)]$ units, in which the Cs^+ ions exist at the midpoints between the [18]crown-6 molecules.

fixed by the [18]crown-6 molecules. Moreover, the Li^+ ions have a large thermal factor along the ionic channel direction; this suggests dynamic translational motion of the ions within the channel. The average $Na^+ \cdots O$ distance (2.75 Å) in the salt **2a** within the [18]crown-6 cavity is ≈0.3 Å longer than the van der Waals contact,[20] while a short $Na^+ \cdots O$ bond length (2.25(1) Å) is found between the Na^+ ion and water oxygen atoms at the axial position. The Cs^+ ions in salt **5** are coordinated by twelve oxygen atoms of the [18]crown-6 molecules above and below the Cs^+ ion. The average $Cs^+ \cdots O$ distance in salt **5** (3.58 Å) is ≈0.4 Å longer than the van der Waals contact (3.21 Å).[20] The large Cs^+ ion cannot pass through the [18]crown-6 cavity and are loosely fixed between two [18]crown-6 molecules.

The common character of the $M^+ \cdots O$ interactions found in the ionic channel structure is the weak coordination of the M^+ ions by the [18]crown-6 molecules and the incomplete site occupation. Among them, the Li^+ ion within the ionic channel has extremely long $M^+ \cdots O$ contacts relative to the others; this suggests dynamic ionic motion within the channel. The distribution as well as the magnitude of motional freedom of each ion within the ionic channel is related to the electrical and magnetic properties of the type **I** salts (see below).

Crystal structure of type II salts: In the case of Li^+ and Na^+ salts, a polymorphism was observed and type **II** salts **1b** and **2b** were obtained in addition to the type **I** salts. The salts **1b** and **2b** contain solvent molecules (CH_3CN and H_2O), which take part in the construction of the SC^+ structures of dimeric $\{(M^+)([18]crown\text{-}6)(CH_3CN)_x(H_2O)_{1.5-x}\}_2$ unit. The SC^+ units are located in the cavities between $[Ni(dmit)_2]$ layers, without intermolecular $M^+ \cdots S$ contacts.

The $[Ni(dmit)_2]$ molecules of the salts **1b** and **2b** are stacked along the *a* and *c* axes, respectively, while the $\{(M^+)_2([18]crown\text{-}6)_2\}$ units stack orthogonally to the stacking axis of the $[Ni(dmit)_2]$ column (Figures 3 and 4). The $[Ni(dmit)_2]$ column of the salt **1b** is composed of the **A-B-C** trimer unit (Figure 3c), and reflects the cation/$[Ni(dmit)_2]$ ratio of 1:3. The strong trimerization is confirmed by the large transfer integrals of $t_1 = 15.17$ and $t_3 = 14.83$. The intertrimer **A**–**C** interaction ($t_2 = -0.89$) is not effective enough to increase the interaction along the stacking direction. In addition, the $[Ni(dmit)_2]$ columns are connected by eight weak intercolumnar interactions along the $a+c$ (t_5, t_7, $t_{4'}$, and t_6) and the $a-3c$ (t_4, t_6, $t_{5'}$, and $t_{7'}$) directions. Among them, the t_5 interaction (2.62) is the most effective. Similar **A-B-C** trimer units are observed in the salt **2b** with transfer integrals of $t_1 = -17.20$ and $t_2 = -16.20$; these are quite significantly larger than that of the intertrimer integral ($t_3 = -0.23$).

$\{(M^+)_2([18]crown\text{-}6)_2\}$ structure: A dimeric structure of $[(Li^+)_2([18]crown\text{-}6)_2(H_2O)_2(CH_3CN)]$ is formed in the salt **1b**, in which two Li^+ ions are connected by a water molecule (O10) (Figure 3a). One of the $\{(Li^+)([18]crown\text{-}6)\}$ units (unit **A**) has a V-shaped conformation, and another water oxygen atom (O9) is located below the molecular plane of the [18]crown-6. Since the ion size of Li^+ is much smaller than the cavity size of [18]crown-6, the Li^+ ion lies on one side within the cavity coordinated by three ether-oxygen atoms, and the noncoordinating part of [18]crown-6 is deformed upwards. In the unit **B**, the Li^+ ion is also coordinated to three oxygen atoms of [18]crown-6, one water oxygen (O10), and the

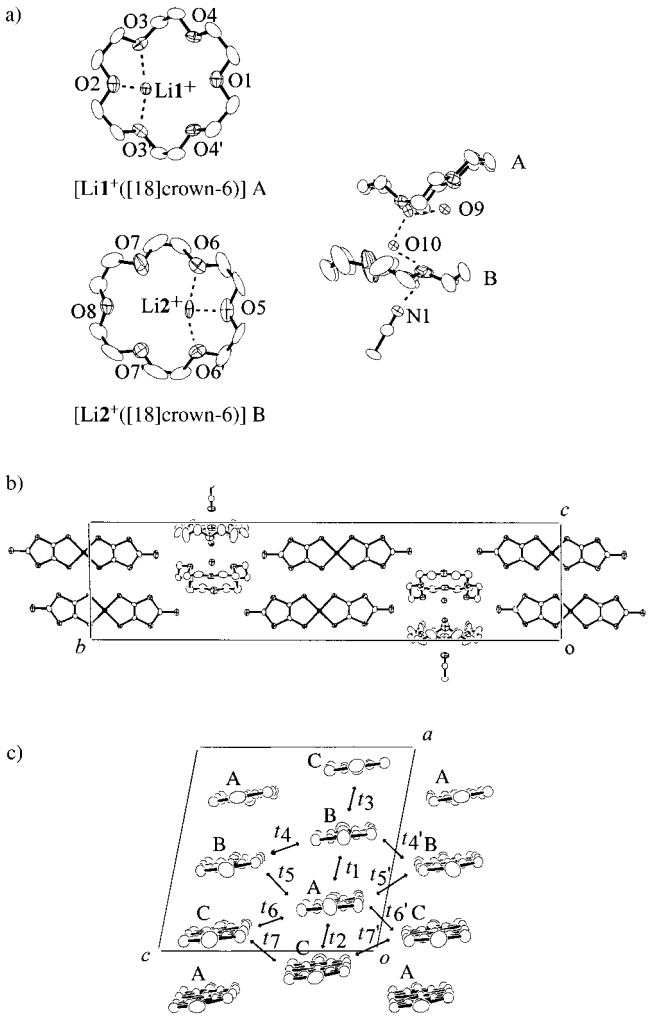

Figure 3. Crystal structure of $[(Li^+)([18]crown\text{-}6)(H_2O)(CH_3CN)_{0.5}][Ni(dmit)_2]_3$ (**1b**). a) Supramolecular cation structures of $[(Li^+)_2([18]crown\text{-}6)_2(H_2O)_2(CH_3CN)]$. Dashed lines indicate the interatomic $Li^+\cdots O$ (N) contacts. b) Unit cell viewed along the *a* axis and c) along the *b* axis.

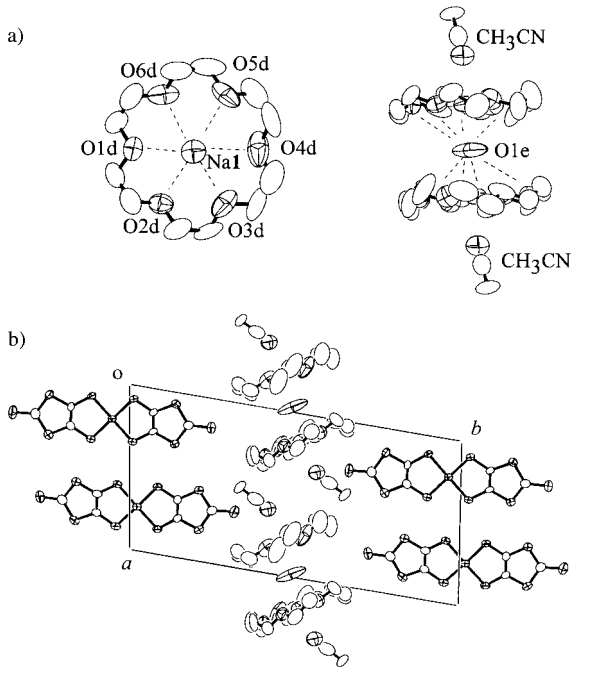

Figure 4. Crystal structure of $[(Na^+)([18]crown\text{-}6)(H_2O)_{0.5}(CH_3CN)][Ni(dmit)_2]_3$ (**2b**). a) Supramolecular cation structure of $[(Na^+)_2([18]crown\text{-}6)_2(H_2O)(CH_3CN)_2]$. Dashed lines indicate the interatomic $Na^+\cdots O$ contacts. b) Unit cell viewed along the *c* axis.

CH_3CN nitrogen (N1) atom. The average bond length between Li^+ and the coordinating oxygen atoms is almost the same as that of the van der Waals contact (2.12 Å).[20] The noncoordinating oxygen sites should be in an environment similar to a free [18]crown-6 molecule. The deformed conformation of [18]crown-6 shows a marked difference compared to the typical disk-shaped conformation observed in the type **I** salt. It is quite natural that the [18]crown-6 molecule should take such a deformed conformation in the crystal when the small Li^+ ion has a van der Waals contact with [18]crown-6 cavity. The planar conformation of [18]crown-6 in the type **I** salt makes the large thermal motion of Li^+ possible within the channel structure.

The Na^+ ions in the salt **2b** are fully included into the [18]crown-6 cavity as in the case of type **I** salt. The $\{Na^+([18]crown\text{-}6)_2(H_2O)\}$ part of the SC^+ structure is similar to the local structure of $\{(Na^+)_x([18]crown\text{-}6)_2(H_2O)\}$ observed in the type **I** salt **2a**. However, the Na^+ ion is further coordinated axially by the CH_3CN molecules; this isolates the SC^+ units from each other as well as from the $[Ni(dmit)_2]$ layers. The bond length of 2.479(4) Å between Na^+ and the water oxygen atom connecting two $\{(Na^+)([18]crown\text{-}6)\}$ units is slightly longer than those in the ionic channel structure. On the other hand, the average $Na^+\cdots O$ distance (2.751 Å) is the same as that in the type **I** salt. Since the Na^+ ions are loosely fixed by the oxygen atoms of [18]crown-6 molecule, the [18]crown-6 molecule has a conformational flexibility in the crystal.

Crystal structure of type III salts: In the cases of K^+ and Rb^+, the ionic channel structure could not be obtained and the type **III** salts of **3** and **4** were formed instead. Since the size of the K^+ and Rb^+ ions corresponds well with that of the [18]crown-6 cavity, they are incorporated stoichiometrically into the cavity of the [18]crown-6 molecule to form typical disc-shape SC^+ structures (Figure 5a).

Figures 5b and c show the unit cell of the salt **3** viewed normal to the $[Ni(dmit)_2]$ plane and along the long axis of the $[Ni(dmit)_2]$ columns, respectively. The **B-A-B′** trimer unit of $[Ni(dmit)_2]$ is stacked along the $-a+c$ axis (Figure 5c). The intradimer and interdimer transfer integrals are -15.3 and -3.70, respectively. In addition, four kinds of intercolumnar interactions are observed along the *c* axis ($t_3 = 3.55$ and $t_5 = 1.32$) and the $2a+c$ axis ($t_4 = -0.06$ and $t_6 = -0.67$) (Figure 5c). The salt **4** has the same intermolecular interactions (Table 2). Since the intratrimer transfer integrals of the type **III** salts are of almost the same magnitude as those found in the type **II** salts, the strong trimerization within the $[Ni(dmit)_2]$ column is a common structural character of the type **II** and **III** salts.

$[(M^+)([18]crown\text{-}6)]$ structure: The cavity size (1.3 – 1.6 Å) of [18]crown-6 corresponds to the ionic radii of K^+ (1.33) and Rb^+ (1.48 Å).[21] The K^+ and Rb^+ ions are included at the

0947-6539/01/0722-4906 $ 17.50+.50/0 *Chem. Eur. J.* **2001**, *7*, No. 22

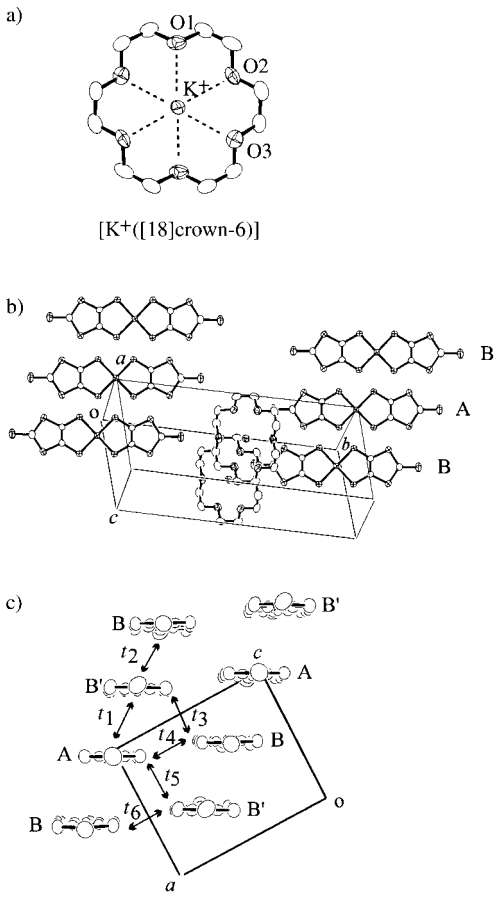

Figure 5. Crystal structure of $[(K^+)([18]crown\text{-}6)][Ni(dmit)_2]_3$ (**3**). a) Supramolecular cation unit of $[(K^+)([18]crown\text{-}6)]$. Dashed lines indicate the interatomic $K^+\cdots O$ contacts. b) Unit cell viewed normal to the $[Ni(dmit)_2]$ plane and c) along the long axis of the $[Ni(dmit)_2]$ molecule.

center of the [18]crown-6 cavity and are coordinated by six oxygen atoms of [18]crown-6 (Figure 5a). The tight coordination of K^+ and Rb^+ ions by the [18]crown-6 molecule is confirmed by the short $M^+\cdots O$ distances. The average $K^+\cdots O$ distance (2.80 Å) in the salt **3** is almost the same as that found in the $[(K^+)([18]crown\text{-}6]SCN^-$ salt (2.805 Å) and is 0.05 Å shorter than the van der Waals contact (2.85 Å).[22] The average $Rb^+\cdots O$ distance of the salt **4** (2.86 Å) is ≈0.14 Å shorter than the van der Waals contact (3.00 Å).[20] The conformation of the [18]crown-6 molecule is fixed by six $M^+\cdots O$ contacts.

The nearest-neighbor M^+-M^+ distance between the $[(M^+)([18]crown\text{-}6)]$ units is quite long (>7 Å); thus, these units are completely isolated from each other. On the other hand, weak contacts between the M^+ ion and the terminal sulfur atoms of the $[Ni(dmit)_2]$ are observed (**3**: 3.420 and **4**: 3.522 Å). A strong $K^+\cdots NC$ contact in the TCNQ salts has been observed in $[(K^+)([18]crown\text{-}6)][TCNQ^-]$,[14] which also conatins an isolated $[(K^+)([18]crown\text{-}6)]$ structure in the crystal. The magnitude of the M^+-S interactions in the $[Ni(dmit)_2]$ salts is much smaller than the M^+-NC interaction of the TCNQ salt due to the smaller negative charge on the terminal sulfur of the $[Ni(dmit)_2]$ molecule. The $M^+\cdots S$ contacts isolates the SC^+ structure and prevents the formation of ionic channel structure.

Flexibility of SC^+ structure in the crystal: The flexibility of $[(M^+)_x([18]crown\text{-}6)]$ structures can be evaluated from the linewidth in the vibrational spectra in addition to the isotropic thermal parameters in X-ray structural analysis. Since the mixed-valence $[Ni(dmit)_2]$ salt has a broad CT band over the IR region, the intense asymmetric C-O-C stretching mode (ν^a_{COC}) is useful to monitor the [18]crown-6 molecules in the crystal.[23] It has been reported that the formation of an $[(M^+)([18]crown\text{-}6)]$ complex causes a slight red-shift (1–2 cm^{-1}) of the ν^a_{COC} mode.[23] The amount of energy shift of the ν^a_{COC} modes in the type **I** and **II** salts is not clear because of the to the broad line shape, while red-shifts of 4–8 cm^{-1} for the ν^a_{COC} mode are observed in the type **III** salts in addition to the sharpening of the band (Figure 6). The origin of the red-shift is the weakening of the C–O bonds on tight complexation of K^+ and Rb^+ ions by the [18]crown-6 molecule.[23a]

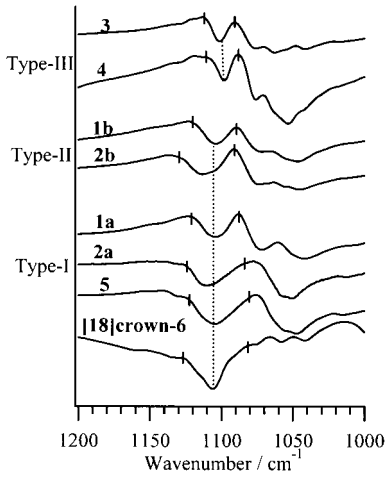

Figure 6. IR spectra of the salts **1a**–**5** and free [18]crown-6 molecule in the region of asymmetric COC stretching mode of [18]crown-6.

The broad vibrational band in [18]crown-6 molecules is related to the flexible molecular motion.[24] Since the free [18]crown-6 molecule has a disorder even at 120 K,[25] the conformation around the C-O-C bonds strongly fluctuates at room temperature. The broad linewidth of the ν^a_{COC} modes found in the type **I** and **II** salts indicates thermally fluctuating $[(M^+)([18]crown\text{-}6)]$ structures that are in an environment close to that of a free [18]crown-6 molecule. In the type **III** salts, K^+ and Rb^+ ions are tightly bound to the [18]crown-6 cavity; this reduces the molecular motion of [18]crown-6 resulting in a narrow linewidth of the $\tilde{\nu}^a_{COC}$ modes.

The average isotropic thermal parameter (B) of oxygen atoms and M^+ ions are also in good agreement with the thermally fluctuating SC^+ structures in the type **I** and **II** salts (Table 2). The B values found in the type **I** and **II** salts are larger than those of type **III** salts. The tight coordination of the [18]crown-6 molecule to the K^+ and Rb^+ ions decreases the magnitude of the B values of the $[(M^+)([18]crown\text{-}6)]$ units in the type **III** salts.

Electrical conductivity: The electrical and magnetic properties of the salts **1a**–**5** are summarized in Table 3. The conductivities at 300 K ($\sigma_{300\,K}$) of the type **I** salts (10–

Table 3. Electrical conductivities at room temperature (σ_{RT}), activation energy (E_a), and magnetic susceptibility (χ_m) of the salts **1**–**5**.

	Type	σ_{RT}[a] [S cm^{-1}]	E_a [eV]	$\chi_{m(300\,K)}$ [emu mol^{-1}]
1a	**I**	11.2	M[b]	2.8×10^{-4}
2a	**I**	12.0	M[b]	10.8×10^{-4}
5	**I**	17.0	M[b]	9.9×10^{-4}
1b	**II**	0.6	0.15[c]	–
2b	**II**	0.06	0.40	–
3	**III**	0.08	0.28[c]	–
4	**III**	0.2	0.36[c]	–

[a] Measured by the standard four-probe d.c. method. [b] Metallic. [c] The activation energies E_a of salts **1b**, **3**, and **4** were obtained in the temperature regions above 230 K.

30 S cm^{-1}) are higher by two orders of magnitude than those of the type **II** and **III** salts (0.06–0.6 S cm^{-1}). The type **II** and **III** salts show semiconducting behavior, and, except for salt **2b**, exhibit a semiconductor–semiconductor transition at $\approx$230 K. The electrical conducting behavior of the type **II** and **III** salts reflects the strongly trimerized [Ni(dmit)$_2$] structure in the electrically conducting columns.

The highly conducting character of type **I** salts arises from the uniform stacking structure of the [Ni(dmit)$_2$] column. Figure 7 shows the temperature-dependent resistivity (ρ) of

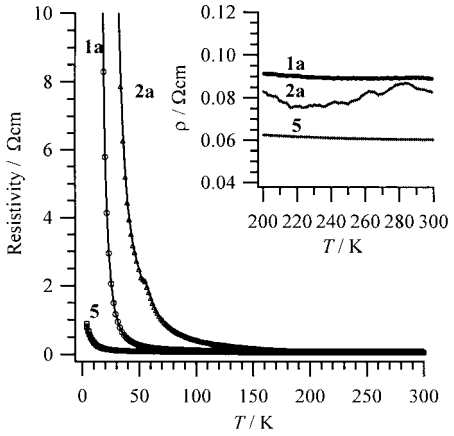

Figure 7. Temperature-dependent electrical resistivity of the type **I** salts (**1a**, **2a**, and **5**). Inset shows the plot in the temperature range from 200 to 300 K.

the type **I** salts. The resistively is almost temperature independent in the high-temperature region (inset in the Figure 7) and the semiconducting behavior (negative slope in the resistivity vs. temperature curve) becomes dominant at lower temperature for the salts **1a** and **2a**. The $\rho_{10\,K}/\rho_{300\,K}$ values of the salts **1a** and **2a** are 1400 and 2600, respectively, while the salt **5** maintained high conductivity down to 10 K ($\rho_{4\,K}/\rho_{300\,K} =$ 10). The activation energies of the salts **1a**, **2a**, and **5** in the semiconducting region are 16, 44, and 4×10^{-3} eV, respectively.

The type **I** salts have the same band structure, and the conduction electrons in the [Ni(dmit)$_2$] column should have a Fermi surface in the quasi one-dimensional band within the tight-binding approximation. However, the highly one-dimensional electronic structure of the type **I** salts is sensitive to the static disorder or dynamic motion of the countercation within the ionic channel. The magnetic measurements showed that the semiconducting behavior of salt **2a** should be explained by the static positional disorder of the Na^+ ions within the ionic channel, while the electrical conductivity of salt **1a** should be discussed in terms of thermally induced ionic motion and their freezing at low temperature, as in the case of the $[(Li^+)_{0.6}([15]\text{-crown-5})(H_2O)][Ni(dmit)_2]_2$ salt previously reported.[17] On the other hand, the salt **5** is essentially a one-dimensional metal. These results are discussed in the next section.

Magnetic susceptibility of type I salts: Figure 8 shows the temperature-dependent magnetic susceptibility (χ_m) per two [Ni(dmit)$_2$] units of the type **I** salts. Although the [Ni(dmit)$_2$]

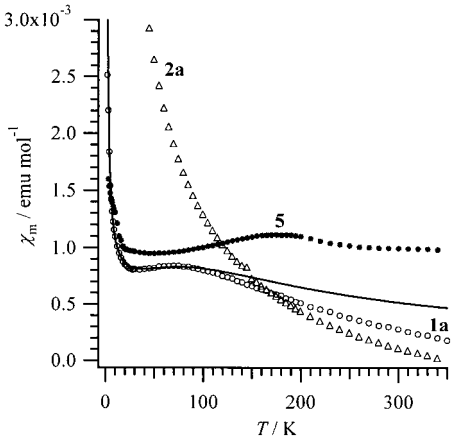

Figure 8. Temperature-dependent magnetic susceptibility (χ_m) per two [Ni(dmit)$_2$] units of type **I** salts. The solid line is a fit of the one-dimensional linear antiferromagnetic Heisenberg chain model for the salt **1a**.

arrangements are the same for the type **I** salts, the magnetic behavior of the Li^+, Na^+, and Cs^+ salts are completely different to one another. The salts **1a** and **5** have small χ_m maxima in the plot of χ_m against T, while the χ_m of salt **2a** increased steadily as the temperature decreased.

The temperature-dependent magnetic susceptibility of salt **2a** is well explained by the one-dimensional disordered antiferromagnetic Heisenberg chain model. This model is based on a probability distribution of the exchange energy J in random magnetic interaction.[26] A canonical transformation reduces the temperature dependent χ_m behavior [Eq. (19].

$$\chi_m \propto \frac{1}{T^{1-c}} \quad (1)$$

The magnetic behavior of salt **2a** is well reproduced with the fitting parameter $c = 0.27$. The temperature-dependent χ_m behavior of salt **2a** is similar to that of [*N*-methylphenazinium][TCNQ].[26] The origin of localized spins of salt **2a**, despite the high electrical conductivity, results from the static disorder of Na^+ ions within the ionic channel; this generates the nonperiodical potential field in the crystal and acts as a source of pinning potential for conduction electrons within the one-dimensional [Ni(dmit)$_2$] column. The randomly occupied spins on regular [Ni(dmit)$_2$] columns of salt **2a**

0947-6539/01/0722-4908 $ 17.50+.50/0 *Chem. Eur. J.* **2001**, *7*, No. 22

induce the probability distribution of magnetic interaction J, which should be directly related to the Na^+ distribution within the ionic channel.

The χ_m value of salt **1a** below 100 K is consistent with the one-dimensional linear antiferromagnetic Heisenberg chain model[27] after subtracting the 1.4% Curie component of $S = 1/2$ spin. The magnetic exchange energy (J/k_B) and spin number below 100 K are -62 K and 0.42 spin ($g \sim 2$) per two $[Ni(dmit)_2]$ units, respectively (solid line in Figure 8). Deviation from the one-dimensional linear antiferromagnetic Heisenberg chain model is observed above 100 K. The behavior closely resembles that of $[(Li^+)_{0.6}([15]crown\text{-}5)(H_2O)][Ni(dmit)_2]_2$, the deviation from the one-dimensional linear Heisenberg chain model of this salt was explained by the contribution from Pauli paramagnetism.[17] The gradual transition from the localized Heisenberg antiferromagnetic state to the metallic Pauli paramagnetic state at higher temperatures is explained as follows: The small sized Li^+ ion can pass through the cavity of [18]crown-6, thus ionic motion is possible in the salt **1a**. Upon lowering the temperature, the translational Li^+ motion gradually freezes and the Li^+ arrangement is fixed within the ionic channel. The quasi one-dimensional electronic band of $[Ni(dmit)_2]$ is strongly affected by such ionic motion. The random potential of the ionic lattice generated by the freezing of the Li^+ ion should localize the electrons on the highly one-dimensional conduction band and open an energy gap at the Fermi surface of the $[Ni(dmit)_2]$ column; this results in the one-dimensional antiferromagnetic Heisenberg behavior of electronic system. On the other hand, the dynamic Li^+ motion averages the random potential field and suppresses the band-gap formation. Thus, metallic behavior becomes evident at higher temperatures. It is not clear at present, however, why the Li^+ salt exhibits ordinary one-dimensional antiferromagnetic behavior in the low-temperature phase rather than a disordered antiferromagnetic behavior as seen in the Na^+ salt.

The deviation from the Pauli paramagnetic state in salt **1a** occurs at a much lower temperature (100 K) relative to the $[(Li^+)_{0.6}([15]crown\text{-}5)(H_2O)][Ni(dmit)_2]_2$ salt (200 K); this is related to the degree of motional freedom of Li^+ ions within the ionic channel. Since the minimum cavity size of [18]crown-6 is ≈ 0.4 Å larger than that of [15]crown-5, the Li^+ ions within the ionic channel of [18]crown-6 have a larger motional freedom than those in [15]crown-5. The solid-state ^7Li NMR measurement suggested that the dynamic Li^+ motion in the salt **1a** is maintained down to the temperature at which the deviation from the one-dimensional linear antiferromagnetic Heisenberg chain model is observed.[28]

The absolute χ_m value of salt **5** in the temperature range from 10 K to 350 K is slightly larger than that expected from the Pauli paramagnetism ($\approx 10^{-4}$ emu mol^{-1}). The enhanced susceptibility indicates a very localized character of the conduction electrons similar to that observed in the metallic $(CH_3)_4N[Ni(dmit)_2]_2$ and α-$[(CH_3)_2(C_5H_{10})N][Ni(dmit)_2]_2$ salts.[29] The appearance of a broad χ_m maximum in the Pauli paramagnetism has been reported in the α-$[(CH_3)_2(C_5H_{10})N][Ni(dmit)_2]_2$ salt; this is attributed to the antiferromagnetic interaction within the metallic state.[29b] Thus, we can safely conclude from the magnetic properties that the salt **5** is a metal. The high room-temperature conductivity and the semiconducting behavior at lower temperatures together with the extremely small activation energy indicate that salt **5** should be categorized as a "disordered metal". Because of the highly one-dimensional electronic structure of the salt **5**, electronic conduction is easily disrupted by the random distribution of the Cs^+ ions in the ionic channel structure.

The electronic state of salt **5** resembles that of the KCP salts, $K_2Pt(CN)_4X_{0.3} \cdot n(H_2O)$, in which the halogen ion X^- is nonstoichiometrically incorporated in the crystal. As in the case of KCP salts,[30] the salt **5** exhibits a diffuse streak at $0.2a^*$ in the Laue photograph at 297 K along the stacking direction. The diffuse streak becomes a superstructure at ≈ 100 K. The streak corresponds to the $2k_F$ periodicity in the $[Ni(dmit)_2]$ column; this is a further indication of the metallic state of the salt **5**.

Although the structure of the $[Ni(dmit)_2]$ column in salts **1a**, **2a**, and **5** are the same, the counterion distribution in the ionic channel structure completely changes the electronic and magnetic properties of the $[Ni(dmit)_2]$ column; this further indicates a possibility for controlling the electronic state through the design of an ionic channel structure.

Formation of ionic channel structure: We will discuss the origin of the SC^+ structures in terms of the complex formation between the M^+ ion and the [18]crown-6 molecule in solution. The equilibrium constant K_c for the $[M^+([18]crown\text{-}6)]$ complex formation proved to be one of the useful parameters in controlling the types of SC^+ structures found in the crystal.

Figure 9 shows the $\log K_c$ versus ionic radius plots for [18]crown-6 and alkali metal cations. The $\log K_c$ values are mainly governed by the balance of the ionic radius and the

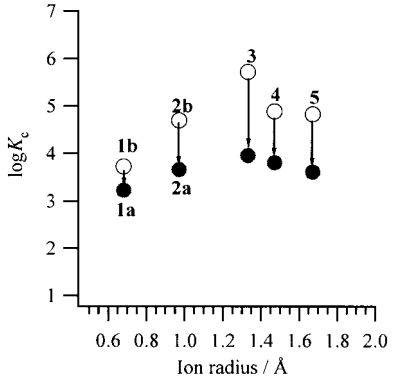

Figure 9. The complex formation constant ($\log K_c$) versus ionic radius of Li^+ (0.6 Å), Na^+ (0.95 Å), K^+ (1.33 Å), Rb^+ (1.48 Å), and Cs^+ (1.69 Å). The open and closed circles are data in CH_3CN (Refs. [34, 35, 38]) and CH_3CN/H_2O (9:1, this work), respectively.

cavity size of crown ethers. The large $\log K_c$ values of 5.72 and 4.89 for K^+ and Rb^+, respectively, in CH_3CN reflected the fact that the ionic radii of the K^+ and Rb^+ fit well into the cavity of [18]crown-6 molecule.[31] Under electrocrystallization conditions, K^+ and Rb^+ ions are tightly included into the [18]crown-6 cavity in CH_3CN to form typical disc-shaped SC^+ struc-

tures,[22] which are incorporated into the cavities between the $[Ni(dmit)_2]$ layers in the type **III** crystal.

The $\log K_c$ values of Li^+ and Na^+ ions against [18]crown-6 in CH_3CN have been reported to be 3.73 and 4.7, respectively.[32] The Li^+ and Na^+ ions are also coordinated by oxygen atoms of [18]crown-6 in solution. The Li^+ and Na^+ ions are too small to form six effective $M^+ \cdots O$ contacts within the [18]crown-6 cavity, and the ions are further solvated by CH_3CN molecules. Since the solvation ability of a water molecule to the Li^+ and Na^+ ions is higher than that of CH_3CN,[33] low contamination with water molecules in the electrocrystallization solvent will lead to the water-containing SC^+ structures, such as $[(Li^+)_2([18]crown\text{-}6)_2(H_2O)_2(CH_3CN)]$ and $[(Na^+)_2([18]crown\text{-}6)_2(H_2O)(CH_3CN)_2]$, in which two M^+ ions are bridged by a H_2O molecule. It seems that these SC^+ structures are directly incorporated into the crystal to give type **II** salts.

Two kinds of complex formation processes, $\log K_c(1) = 4.83$ and $\log K_c(2) = 0.57$, have been reported for the $[(Cs^+)_x([18]crown\text{-}6)]$ adducts in CH_3CN.[34] The two processes correspond to the complex formation of the $[(Cs^+)([18]crown\text{-}6)]$ and $[(Cs^+)([18]crown\text{-}6)_2]$ species, respectively. Since the Cs^+ ion is much larger than the cavity of [18]crown-6, the ions are located outside of the [18]crown-6 plane in $[(Cs^+)([18]crown\text{-}6)]$ and are further coordinated by another [18]crown-6 to give the sandwich structure of $[(Cs^+)([18]crown\text{-}6)_2]$. These species will form an infinite $[(Cs^+)_x([18]crown\text{-}6)]_\infty$ chain through $M^+ - O$ interactions, which should be the origin of the ionic channel structure in the salt **5**. The 6:1 ratio of the $[(Cs^+)([18]crown\text{-}6)]$ and $[(Cs^+)([18]crown\text{-}6)_2]$ units provides a stoichiometry close to $[(Cs^+)_{0.8}([18]crown\text{-}6)]$ observed in the salt **5**.

To realize the ionic channel structure in the crystals of Li^+, Na^+, K^+, or Rb^+, we first have to destroy the ion-capturing SC^+ structures already formed in solution. The addition of the H_2O into CH_3CN solution decreases the cation binding ability through hydrogen-bond formation between M^+ ions and water molecules.[32b][35, 36] The decrease of the $\log K_c$ value upon the addition of water to the CH_3CN solution was confirmed by the conductometry measurements. The $\log K_c$ values of the Li^+, Na^+, K^+, Rb^+, and Cs^+ ions in CH_3CN/H_2O (9:1) are 3.23, 3.67, 3.96, 3.81, and 3.61, respectively (Figure 9). The solvation of water molecules destroys or rearranges the SC^+ structure in solution.

In the case of the Na^+ salt, the local SC^+ structure of $[(Na^+)_x([18]crown\text{-}6)_2(H_2O)]$ is almost the same for the salts **2a** and **2b**, except that the amount of Na^+ is less than unity in the former case. By the introduction of a large amount of water molecules in the electrocrystallization solution, the $[(Na^+)_x([18]crown\text{-}6)_2(H_2O)]$ units are connected to each other to form infinite $[(Na^+)_x([18]crown\text{-}6)(H_2O)]_\infty$ chains. It seems that the ionic channel structures are rather subtle and the regular stack is retained, even if a significant amount of vacant sites exists. The amount of the ions in the crystal is determined according to the oxidation state of $[Ni(dmit)_2]$ (or the amount of conduction electrons on the $[Ni(dmit)_2]$ column) and vice versa.

The ionic channel structure of the Li^+ salt is quite unusual, if it is compared with that of the type **II** salt, in which the [18]crown-6 is largely deformed to include Li^+ ion into the cavity. Although the hydration energy of Li^+ is much larger than that of Na^+,[37] the water molecules are not included in the ionic channel structure. It should be noted that the ionic channel structure observed in $[(Li^+)_{0.6}([15]crown\text{-}5)(H_2O)][Ni(dmit)_2]_2$ has water molecules at the inversion center between two adjacent [15]crown-5 molecules. At present, we ascribe the formation of the ionic channel structure in the salt **1a** without water molecules to the large thermal motion of the Li^+ ions in the ionic channel; this should eliminate the water molecules upon the formation of the [18]crown-6 stack and keep the $[(Li^+)_x([18]crown\text{-}6)]_\infty$ infinite chain structure through the weak contacts of Li^+ ions with oxygen atoms of [18]crown-6.

Although further experimental evidence is necessary to clarify the detailed process of the ionic channel formation, the design of the ionic channel structure is possible by tuning the K_c values under electrocrystallization conditions.

Conclusion

The supramolecular cation (SC^+) units, which are composed of alkali metal ions ($M^+ = Li^+$, Na^+, K^+, Rb^+, and Cs^+) and [18]crown-6 molecules, are incorporated into highly conducting $[Ni(dmit)_2]$ salts. The crystals are classified into three types (**I**, **II**, and **III**) based on the SC^+ structures. The type **I** salts ($M^+ = Li^+$, Na^+, and Cs^+) have an ionic channel structure in which the $[(M^+)_x([18]crown\text{-}6)]$ units are assembled in an infinite regular array through the $M^+ - O$ interactions, while type **II** ($M^+ = Li^+$ and Na^+) and type **III** salts ($M^+ = K^+$ and Rb^+) have isolated SC^+ structures. Since the $M^+ - O$ interactions found in the ionic channel are of significant weakness, the M^+ ions are not fixed tightly within the channel and possibly have a translational freedom in the case of the Li^+ salt.

The $[Ni(dmit)_2]$ columns of the type **II** and **III** salts are composed of trimer units, while the type **I** salts have a uniform stack. The electrical conductivities of the type **I** salt at room temperature are two orders of magnitude higher than those of the type **II** and **III** salts. The type **I** salts have a one-dimensional Fermi surface within the tight-binding approximation. However, the electronic properties of the salts are strongly influenced by the distribution and the dynamic motion of ions within the channel, the amount of which is nonstoichiometric in the crystal. The Na^+ salt exhibits semiconducting behavior and the magnetic properties are described by the one-dimensional disordered antiferromagnetic Heisenberg chain, on account of the random distribution of Na^+ ions within the ionic channel. On the other hand, a gradual metal – insulator transition is observed in the Li^+ salt. This is associated with the dynamic ionic motions within the ionic channel and their freezing at low temperature. The Cs^+ salt showed an essentially metallic behavior exhibiting $2k_F$ diffuse-scattering characteristics of a quasi one-dimensional metal.

The regulation of the ionic motion by changing the strength of the $M^+ - O$ interactions is interesting from the viewpoint of controlling the conduction electrons. Changing the crown ether from an 18-membered ring to a 24-membered ring or to other heterocrown ethers, such as thia-crown and aza-crown

0947-6539/01/0722-4910 $ 17.50+.50/0 *Chem. Eur. J.* **2001**, *7*, No. 22

ethers, should modulate the strength of $M^+ - O$ interactions and thus the degree of the electron localization. The higher valence M^{2+} and M^{3+} ions should also increase the electron localization potential. Another possibility is the control of the number of vacant sites, that is, the control of the number of conduction electrons in the π bands.

Finally, the equilibrium constant (K_c) between the M^+ ions and the [18]crown-6 molecule in the electrocrystallization solvent is a useful parameter for designing the ionic channel structures in [Ni(dmit)$_2$]-based molecular conductors. The ionic channel-type SC^+ structures are preferentially formed by the addition of a polar solvent, such as water, to the electrocrystallization solvent by reducing the K_c values. The next step should be the construction of highly conducting systems for both ions and electrons and introduction of mobile magnetic ions into the channel, by the formation of ionic channel structures in molecular conductors and magnets.

Experimental Section

General: The measurement of IR spectra ($\nu = 400 - 7600$ cm^{-1}) was carried out on KBr pellet samples by using a Perkin–Elmer Spectrum 2000 spectrophotometer with a resolution of 1 cm^{-1}. Acetonitrile (CH_3CN) was distilled from calcium hydride under argon atmosphere prior to use. The complex formation constants (K_c) between the alkali metal ions and [18]crown-6 in $CH_3CN/CH_3CN/H_2O$ (9:1) were determined by the conductometry.[38] A conductance cell (CT-57101B, TOA Electronics Ltd.) was employed in the titration procedure of $MClO_4$ (0.1 mM) by [18]crown-6 (0–1 mM) at 24 °C.

Preparation of [Ni(dmit)$_2$] salts: The monovalent (nBu$_4$N)[Ni(dmit)$_2$] salt was prepared according to the literature.[39] The crystals were grown using the standard electrocrystallization method. Supporting electrolytes ($LiClO_4 \cdot 3H_2O$, $NaClO_4$, $KClO_4$, $RbClO_4$, and CsI) were recrystallized from CH_3CN or H_2O, then dried in vacuum. CH_3CN or CH_3CN/H_2O (9:1) were used as electrocrystallization solvents. A constant current (1 μA) was applied to the platinum electrodes (1 mm$\varnothing$) in an H-shaped cell (18 mL) for two weeks at room temperature. The stoichiometries of the crystals were determined by X-ray structural analyses. In the cases of the Li^+ and Na^+ salts, two kinds of crystal phases were obtained, needle or plate, depending on the electrocrystallization conditions.

Crystal structure determinations: Crystal data were collected on a Rigaku AFC-5R or AFC-7R diffractometer with $Mo_{K\alpha}$ ($\lambda = 0.71073$ Å) radiation and a graphite monochromator. The unit cell parameters were determined and refined from 25 reflections. Data were collected with ω scan for the salts **1a**, **2a**, and **5** or $2\theta - \omega$ scan for the salts **1b**, **2b**, **3**, and **4** with maximum 2θ of 55.0°. Lorentz polarization and absorption corrections applied in the refinements. The structure refinements were performed by the full-matrix least-squares method. Calculations were performed by using teXsan crystallographic software packages.[40] The crystal data are summarized in Table 4. Parameters were refined with the anisotropic temperature factors in all crystals, and the hydrogen atoms were removed from the refinements. The occupancies of each M^+ ion were refined in the final stages. A unit occupation of the Li^+, Na^+, K^+, and Rb^+ ions was confirmed in the salts **1b**, **2b**, **3**, and **4**, while the occupancy of the Na^+ and Cs^+ ions in the salts **2a** and **5** were 0.66 and 0.8, respectively. The occupancy factor of the Li^+ ion in the salt **1a** could not be determined from the X-ray analysis on account of the small electron density of the Li^+ ion. Crystallographic data (excluding structure factors) for the structures reported in this paper have been deposited with the Cambridge Crystallographic Data Centre as supplementary publication nos. CCDC-155155 to CCDC-155161. Copies of the data can be obtained free of charge on application to CCDC, 12 Union Road, Cambridge CB2 1EZ, UK (fax: (+44) 1223-336-033; e-mail: deposit@ccdc.cam.ac.uk).

Electrical conductivity: The temperature-dependent electrical conductivity was measured by the dc four-probe method along the long axis of the crystal. The stacking direction of the [Ni(dmit)$_2$] molecules was consistent with the long axis of the crystal. Electrical contacts of gold wire (10 $\mu\varnothing$) to the crystals were made by gold paste (Tokuriki 8560).

Magnetic susceptibility: The temperature-dependent magnetic susceptibility was measured with a SQUID magnetometer (Quantum Design Model MPMS-5) for polycrystalline samples. The magnetic field applied was 1 T for all measurements.

Calculation of transfer integrals and band structures: The transfer integrals (t) and band structures were calculated within the tight-binding approximation with the extended Hückel molecular orbital calculation. The LUMO of the [Ni(dmit)$_2$] molecule was used as the basis function.[41] The semiempirical parameters for Slater-type atomic orbitals were taken from Ref. [41]. The t value between each pair of molecules was assumed to be proportional to the overlap integral (S), $t = -10\,S$ eV. The LUMO band of [Ni(dmit)$_2$] in the type **I** salts was assumed to be quarter-filled for band-structure calculations.

Acknowledgements

This work was partly supported by a Grant-in-Aid for Science Research from the Ministry of Education, Science, Sports, and Culture of Japan and by the Proposal-Based New Industry Creative Type Technology R&D Promotion Program from the New Energy and Industrial Technology Development Organization (NEDO) in Japan. The authors thank Dr. M. Wakeshima and Prof. Y. Hinatsu for the use of the SQUID magnetometer.

Table 4. Crystal data, data collection, and refinement parameters of the salts **1**–**5**.

	1a	**1b**	**2a**	**2b**	**3**	**4**	**5**
formula	$C_{24}H_{24}O_6S_{20}Ni_2Li$	$C_{31}H_{27.5}LiNi_3S_{30}O_7N_{0.5}$	$C_{24}H_{26}O_7S_{20}Ni_2Na$	$C_{32}H_{27}O_7S_{30}Ni_3NaN$	$C_{30}H_{28}O_6S_{30}Ni_3K$	$C_{30}H_{28}O_6S_{30}Ni_3Rb$	$C_{24}H_{26}O_6S_{20}Ni_2Cs$
M_r	1173.99	1663.90	1208.05	3382.93	1657.51	1707.92	1299.96
crystal system	monoclinic	monoclinic	monoclinic	triclinic	triclinic	triclinic	monoclinic
space group	$P2_1/c$	$P2_1/m$	$P2_1/n$	$P\bar{1}$	$P\bar{1}$	$P\bar{1}$	$P2_1/n$
crystal size [mm^3]	0.6 × 0.05 × 0.05	0.5 × 0.13 × .013	0.6 × 0.1 × 0.1	0.6 × 0.2 × 0.1	0.5 × 0.3 × 0.05	0.4 × 0.3 × 0.1	0.5 × 0.05 × 0.05
a [Å]	4.49(2)	11.17(2)	4.503(4)	12.632(2)	8.964(2)	8.971(3)	4.44(1)
b [Å]	11.39(2)	45.78(1)	11.347(5)	24.041(9)	21.773(1)	21.859(5)	11.39(1)
c [Å]	42.84(1)	11.710(4)	43.29(1)	11.236(4)	7.481(1)	7.455(2)	43.496(7)
α [°]				98.14(3)	99.50(2)	99.22(3)	
β [°]	91.6(2)	101.19(5)	89.71(7)	114.52(2)	93.30(1)	93.41(3)	90.96(9)
γ [°]				79.71(3)	94.82(2)	94.44(3)	
V [Å^3]	2189(9)	5871(10)	2212(1)	3046(1)	1431.0(5)	1437.8(7)	2199(3)
Z	2	4	2	2	1	1	2
ρ_{calcd} [g cm^{-3}]	1.781	1.882	1.831	1.852	1.923	1.976	1.963
T [K]	296	200	296	296	296	296	296
μ [cm^{-1}]	18.51	20.63	18.45	19.97	21.85	29.48	26.59
R[a]	0.149	0.051	0.055	0.051	0.047	0.103	0.055
R_w[a]	0.124	0.041	0.057	0.119	0.044	0.131	0.052

[a] $R = \Sigma||F_o| - |F_c||/\Sigma|F_o|$ and $R_w = (\Sigma\omega(|F_o| - |F_c|)^2/\Sigma\omega F_o^2)^{1/2}$.

[1] a) B. Albert, D. Bray, A. Johnson, J. Lewis, M. Raff, K. Roberts, P. Walter, *Molecular Biology of the Cell*, Garland Publishing, New York, **1994**; b) L. Stryer, *Biochemistry*, W. H. Freeman, New York, **1995**.

[2] B. Hille, *Ionic Channels of Excitable Membranes*, Sinauer Associates, Sunderland, **1992**.

[3] a) K. S. Åkerfeldt, J. D. Lear, Z. R. Wasserman, L. A. Chung, W. F. DeGrado, *Acc. Chem. Res.* **1993**, *26*, 191; b) K. S. Åkerfeldt, R. M. Kim, D. Camac, J. T. Groves, J. D. Lear, W. F. DeGrado, *J. Am. Chem. Soc*. **1993**, *26*, 191; c) M. R. Ghadiri, J. R. Granja, L. K. Buehler, *Nature*. **1994**, *369*, 301.

[4] a) G. W. Gokel, O. Murillo, *Acc. Chem. Res.* **1996**, *29*, 425; b) J.-C. Meillon, N. Voyer, *Angew. Chem.* **1997**, *109*, 1004; *Angew. Chem. Int. Ed. Engl*. **1997**, *36*, 967; c) O. Murillo, I. Suzuki, E. Abel, C. L. Murray, E. S. Meadows, T. Jin, G. W. Gokel, *J. Am. Chem. Soc*. **1997**, *119*, 5540; d) G. W. Gokel, *Chem. Commun*. **2000**, 1.

[5] a) E. Weber, J. L. Toner, I. Goldberg, F. Vögtle, D. A. Laidler, J. F. Stoddart, R. A. Bartsch, C. L. Liotta, *Crown Ethers and Analogs* (Eds.: S. Patai, Z. Rappoport), Wiley, New York, **1989**; b) G. W. Gokel, *Crown Ethers & Cryptands* (Ed.: J. F. Stoddart), RSC, Cambridge, **1994**.

[6] a) A.-C. Dock, D. Moras, *Nature* **1982**, *295*, 526; b) M. Noda, H. Takahashi, T. Tanabe, M. Toyosato, S. Kiyotani, Y. Furutani, T. Hirose, H. Takahashi, S. Inayama, T. Miyata, S. Numa, *Nature* **1983**, *302*, 528; c) J. D. Hartgerink, J. R. Granja, R. A. Milligan, M. R. Ghadiri, *J. Am. Chem. Soc*. **1996**, *118*, 43.

[7] a) J.-M. Lehn, *Supramolecular Chemistry* (Ed.: U. Anton), VCH, Weinheim, **1995**; b) T. Akutagawa, T. Hasegawa, T. Nakamura, *Handbook of Advanced Electronic and Photonic Materials and Devices*, Vol. 3, (Ed.: H. S. Nalwa), Academic Press, San Diego, **2000**, p. 267.

[8] a) D. O. Cowan, *New Aspects of Organic Chemistry* (Eds.: Z. Yoshida, T. Shiba, Y. Oshiro), Kodansha, Tokyo, **1989**; b) *Handbook of Organic Conductive Molecules and Polymers, Vol. 1* (Ed.: H. S. Nalwa), Wiley, **1997**; c) J. M. Williams, J. R. Ferraro, R. J. Thorn, K. D. Carlson, U. Geiser, H. H. Wang, A. M. Kini, M.-H. Whangbo, *Organic Superconductors* (Ed.: R. N. Grimes), Prentice-Hall, New Jersey, **1992**; d) T. Ishiguro, K. Yamaji, G. Saito, *Organic Superconductors*, 2nd ed. (Eds.: M. Cardona, P. Fulde, K. von Klitzing, H.-J. Queisser), Springer, Berlin, **1998**.

[9] a) K. Bechggard, K. Carneiro, M. Olsen, F. B. Rasmussen, C. S. Jacobsen, *Phys. Rev. Lett*. **1981**, *46*, 867; b) J. P. Pouget, G. Shirane, K. Bechgaard, J. M. Fabre, *Phys. Rev. B* **1983**, *27*, 5203; c) S. Kagoshima, T. Yasunaga, T. Ishiguro, H. Anzai, G. Saito, *Solid State Commun*. **1983**, *46*, 867; d) H. Schwenk, K. Andres, F. Wudl, *Phys. Rev. B* **1984**, *29*, 500.

[10] a) C. Bourbonnais, R. T. Henriques, P. Wzietek, D. Kongeter, J. Voiron, D. Jérôme, *Phys. Rev. B* **1991**, *44*, 641; b) G. Bonfait, M. J. Matos, R. T. Henriques, M. Almeida, *J. Phys. IV* **1993**, *3*, 251; c) M. Matos, G. Bonfait, R. T. Henriques, M. Almeida, *Phys. Rev. B* **1996**, *54*, 15307.

[11] E. Coronado, J. R. Galán-Mascarós, C. J. Gómez-Garcia, V. Laukhin, *Nature* **2000**, *408*, 447.

[12] a) H. Kobayashi, A. Sato, E. Arai, H. Akutsu, A. Kobayashi, P. Cassoux, *J. Am. Chem. Soc*. **1997**, *119*, 12392; b) A. Sato, E. Ojima, H. Akutsu, H. Kobayashi, A. Kobayashi, P. Cassoux, *Chem. Lett*. **1998**, 673; c) E. Ojima, H. Fujiwara, K. Kato, H. Kobayashi, H. Tanaka, A. Kobayashi, M. Tokumoto, P. Cassoux, *J. Am. Chem. Soc*. **1999**, *121*, 5581; d) A. Sato, E. Ojima, H. Akutsu, Y. Nakazawa, H. Kobayashi, H. Tanaka, A. Kobayashi, P. Cassoux, *Phys. Rev. B* **2000**, *61*, 111; e) H. Fujiwara, E. Fujiwara, Y. Nakazawa, B. Z. Narymbetov, K. Kato, H. Kobayashi, A. Kobayashi, M. Tokumoto, P. Cassoux, *J. Am. Chem. Soc*. **2001**, *123*, 306.

[13] a) M. Morinaga, T. Nogami, Y. Kanda, T. Matumoto, K. Matsuoka, H. Mikawa, *Bull. Chem. Soc. Jpn*. **1980**, *53*, 1221; b) K. Matsuoka, T. Nogami, T. Matsumoto, H. Tanaka, H. Mikawa, *Bull. Chem. Soc. Jpn*. **1982**, *55*, 2015; c) M. C. Grossel, F. A. Evans, J. A. Hriljac, J. R. Morton, Y. LePage, K. F. Preston, L. H. Sutcliffe, A. J. Williams, *J. Chem. Soc. Chem. Commun*. **1990**, 439.

[14] a) T. Nogami, M. Morinaga, H. Mikawa, H. Nakano, M. Morioka, H. Horiuchi, M. Tokonami, *Bull. Chem. Soc. Jpn*. **1990**, *63*, 2414; b) M. C. Grossel, S. C. Weston, *J. Phys. Org. Chem*. **1992**, *5*, 533.

[15] a) O. E. Sielcken, J. Schram, R. J. M. Nolte, J. Schoonmann, W. Drenth, *J. Chem. Soc. Chem. Commun*. **1988**, 108; b) C. F. Nostrum, R. J. M. Nolte, *Chem. Commun*. **1996**, 2385; c) C. F. Nostrum, *Adv. Mater*. **1996**, *8*, 1027; d) O. E. Sielcken, H. C. A. Lindert, W. Drenth, J. Schoonman, J. Schram, R. J. M. Nolte, *Ber. Bunsenges. Phys. Chem*. **1989**, *93*, 702.

[16] a) T. Akutagawa, T. Nakamura, A. E. Underhill, T. Inabe, *J. Mater. Chem*. **1996**, *7*, 135; b) T. Akutagawa, T. Nakamura, A. E. Underhill, T. Inabe, *Synth. Met*. **1997**, *86*, 1961; c) T. Akutagawa, T. Nakamura, T. Inabe, A. E. Underhill, *Thin Solid Films* **1998**, *331*, 264; d) T. Akutagawa, Y. Nezu, T. Hasegawa, T. Nakamura, K. Sugiura, Y. Sakata, T. Inabe, A. E. Underhill, *Chem. Commun*. **1998**, 2599; e) T. Akutagawa, T. Hasegawa, T. Nakamura, T. Inabe, K. Sugiura, Y. Sakata, A. E. Underhill, *Synth. Met*. **1999**, *102*, 1747; f) T. Akutagawa, T. Nakamura, *Coord. Chem. Rev*. **2000**, *198*, 297; g) T. Akutagawa, T. Hasegawa, T. Nakamura, S. Takeda, T. Inabe, K. Sugiura, Y. Sakata, A. E. Underhill, *Inorg. Chem*. **2000**, *39*, 2645.

[17] T. Nakamura, T. Akutagawa, K. Honda, A. E. Underhill, A. T. Coomber, R. H. Friend, *Nature* **1998**, *394*, 159.

[18] H. Kim, A. Kobayashi, Y. Sasaki, R. Kato, H. Kobayashi, *Chem. Lett*. **1987**, 1799.

[19] L. Brossard, M. Ribault, L. Valade, P. Cassoux, *Phys. Rev. B* **1990**, *42*, 3935.

[20] A. Bondi, *J. Phys. Chem*. **1964**, *68*, 441.

[21] C. Pederson, *Synthetic Multidendate Macrocyclic Compounds* (Eds.: R. M. Izatt, J. J. Christensen), Academic Press, New York, **1978**.

[22] a) J. D. Dunitz, M. Dobler, P. Seiler, R. P. Phizackerley, *Acta. Crystallogr. Sect. B* **1974**, *30*, 2773; b) P. Seiler, M. Dobler, J. D. Dunitz, *Acta. Crystallogr Sect. B* **1974**, *30*, 2744; b) M. Dobler, R. P. Phizackerley, *Acta. Crystallogr Sect. B* **1974**, *30*, 2746.

[23] a) H. Li, T. Jiang, I. S. Butler, *J. Raman Spect*. **1989**, *20*, 569; b) H. Fukuhara, K. Ikeda, H. Matsuura, *J. Mol. Struct*. **1990**, *224*, 203.

[24] P. L. Huyskens, W. A. Luck, *Intermolecular Forces. An Introduction to Modern Method and Results* (Ed.: T. Zeegers-Huyskens), Springer, Heidelberg, **1991**.

[25] J. Dunitz, P. Seiler, *Acta. Crystallogr Sect. B* **1974**, *30*, 2739.

[26] a) G. Theodorou, M. H. Cohen, *Phys. Rev. Lett*. **1976**, *37*, 1014; b) G. Theodorou, *Phys. Rev. B* **1977**, *16*, 2273.

[27] J. C. Bonner, M. E. Fisher, *Phys. Rev. A* **1964**, *3*, 640.

[28] S. Takeda, unpublished data.

[29] a) H. Tajima, A. Takahashi, H. Kuroda, A. Kobayashi, H. Kobayashi, *Mol. Cyrst. Liq. Cryst*. **1996**, *285*, 125; b) A. Kobayashi, A. Sato, H. Kobayashi, *J. Solid State Chem*. **1999**, *145*, 564.

[30] a) H. Nagasawa, *J. Phys. Soc. Jpn*. **1978**, *45*, 701; b) R. Comes, M. Lambert, H. R. Zeller, *Phys. Status Solidi B* **1973**, *58*, 587; c) H. Nagasawa, *Phys. Status Solidi B* **1982**, *109*, 749.

[31] a) Y. Takeda, *Bull. Chem. Soc. Jpn*. **1983**, *56*, 866; b) M. K. Chantooni, G. Roland, I. M. Kolthoff, *J. Solution Chem*. **1988**, *17*, 175; c) I. K. Lednev, R. E. Hester, J. N. Moore, *J. Chem. Soc. Faraday Trans*. **1997**, *93*, 1551.

[32] a) H. P. Hopkins, A. B. Norman, *J. Phys. Chem*. **1980**, *84*,309; b) T. Nakamura, Y. Yumoto, K. Izutu, *Bull. Chem. Soc. Jpn*. **1982**, *55*, 1850.

[33] T. Nakamura, *Bull. Chem. Soc. Jpn*. **1975**, *48*, 1447.

[34] a) E. Mei, A. I. Popov, J. L. Dye, *J. Phys. Chem*. **1977**, *81*, 1677; b) R. D. Boss, A. I. Popov, *Inorg. Chem*. **1986**, *25*, 1747.

[35] a) R. M. Izatt, J. S. Bradshaw, S. A. Nielsen, J. D. Lamb, J. J. Christensen, D. Sen, *Chem. Rev*. **1985**, *85*, 271; b) R. M. Izatt, K. Pawlak, J. D. Bradshaw, R. L. Bruening, *Chem. Rev*. **1991**, *91*, 721.

[36] a) S. Ahrland, *Pure Appl. Chem*. **1979**, *51*, 2019; b) S. Ahrland, *Pure Appl. Chem*. **1982**, *54*, 1451.

[37] D. R. Rosseinsky, *Chem. Rev*. **1965**, *65*, 467.

[38] Y. Takeda, H. Yano, M. Ishibashi, H. Isozumi, *Bull. Chem. Soc. Jpn*. **1980**, *53*, 72.

[39] G. Steinmecke, H. J. Sieler, R. Krimes, E. Hoyer, *Phosphorus Sulfur* **1979**, *7*, 49.

[40] a) *teXsan for Windows: Single crystal structure analysis software. Ver. 1.06*, Molecular Structure Corporation, **1999**; For ORTEP-3 drawing, see: b) L. J. Farrugia, *J. Appl. Crystallogr* **1997**, *32*, 565.

[41] a) A. J. Berlinsky, J. F. Carolan, L. Weiler, *Solid State Commun*. **1974**, *15*, 795; b) R. H. Summerville, R. J. Hoffmann, *J. Am. Chem. Soc*. **1976**, *98*, 7240; c) T. Mori, A. Kobayashi, Y. Sasaki, H. Kobayashi, G. Saito, H. Inokuchi, *Bull. Chem. Soc. Jpn*. **1984**, *57*, 627.

Received: January 9, 2001 [F2993]

  0947-6539/01/0722-4912 $ 17.50+.50/0